Desalination and Water Treatment
www.deswater.com

doi:10.5004/dwt.2019.23356

139 (2019) 23–38
January

The role of fly ash in solar photocatalytic water treatment

Vanja Gilja[a], Zvonimir Katančić[a], Vilko Mandić[a], Igor Peternel[b], Hrvoje Kušić[a,*], Zlata Hrnjak-Murgić[a,**]

[a]*Faculty of Chemical Engineering and Technology, University of Zagreb, Marulićev trg 19, Zagreb, Croatia, email: vgilja@fkit.hr (V. Gilja), katancic@fkit.hr (Z. Katančić), vmandic@fkit.hr (V. Mandić), Tel. +385 1 4597 123, Fax +385 1 4597 143, email: hkusic@fkit.hr (H. Kušić), Tel. +385 1 4597 120, Fax +385 1 4597 142, email: zhrnjak@fkit.hr (Z. Hrnjak-Murgić)*

[b]*Karlovac University of Applied Sciences, Trg Josipa Jurja Strossmayera 9, Karlovac, Croatia, email: ipeternel@vuka.hr (I. Peternel)*

Received 7 May 2018; Accepted 26 October 2018

ABSTRACT

To investigate the possibility of using waste material in the water purification, fly ash (FA0) was modified and built-in within composite TiO_2-FA. In that purpose, titanium dioxide (TiO_2) was prepared *in-situ* by sol–gel synthesis in the presence of FA. The morphology, surface, structure and optical properties of obtained composite were compared to those of pure TiO_2, synthetized by the same procedure as TiO_2-FA. Both photo catalysts were then used in solar driven treatment of reactive azo dye Reactive Red 45 (RR45), exploring the influence of following process parameters: initial pH, photo catalyst dosage and initial RR45 concentrations, on the overall effectiveness. The reusability of TiO_2-FA and TiO_2 has also been explored. Modification of FA0 significantly increased its surface area. Synthetized TiO_2 was highly crystalline and of anatase phase only, regardless the presence of FA. Band gap of TiO_2-FA is slightly lower than that of TiO_2, indicating that composite might have higher activity under solar irradiation. However, it was found that TiO_2 is more effective, except at extreme conditions tested (the lowest pH and highest photo catalyst dosage), presumably because composite had 16 wt% less photo catalytically active component. On the other hand, composite underwent easier separation after the treatment that facilitated its reuse more efficiently.

Keywords: Fly ash; Material synthesis and characterization; TiO_2-based composite; Solar photo catalysis; Water treatment

1. Introduction

Among various types of advanced oxidation processes (AOPs), photo catalytic processes using semi conducting materials, particularly active under solar irradiation, present an effective and low-energy consumption solution for sustainable water treatment. A common semi conducting material used in photo catalytic purposes is titanium (IV) oxide (TiO_2); widely promoted due to: (i) high photo catalytic activity under the incident photon wavelength of $300 < \lambda < 390$ nm, and (ii) multi-faceted functional properties (chemical and thermal stability, and attractive mechanical properties) [1,2]. However, harvesting a broader spectrum of solar irradiation involves the lowering of the band gap of semi conducting material (e.g. TiO_2 has 3.1–3.2 eV) [2], while inhibiting the recombination of photo generated charges. These can be accomplished by: doping with non-metals, incorporation or deposition of noble metals (ions), and material engineering solutions based on composites formation involving various additional constituents (transition metals, carbon nanotubes, dye sensitizers, conductive polymers, graphene (oxide) and semi conducting materials) [3–5]. Another challenges related to the application of photo catalytic treatment are agglomeration during the operation and requirements for the separation of fine nano-sized particles after the treatment. The solution is the immobilization of photo catalytically active material on either fixed (glass plates, alumina sheets, reactor parts) or movable (porous particles of larger size) supports [2,3,6]. In later case, either

*Corresponding author.

natural (e.g. rice husks, natural zeolites, clays) [3,7,8] or artificially/engineered (e.g. synthetic zeolites, polymers, fly ash) [6,9–12]) materials may be applied. Considering the postulates of circular economy, particularly related to the reuse of waste materials, the application of fly ash, a solid waste generated in large quantities in thermal power plants [13], as a potentially valuable material in any aspects of environmental protection is of high interest [14]. Fly ashes pertain to a group of dispersive powders; it has a crystalline structure with the main constituents: alumino-silica, ferriferous glass, quartz and unburned carbon, with spherically shaped particles with sizes of ~20 μm [11–13].

Accordingly, in this study we have investigated the application of fly ash as an appropriate TiO_2 carrier, as well as its potential as a co-catalyst in solar driven photo catalytic water treatment. In such manner, the waste (fly ash) would be recycled into a value-added product, as of utmost importance in the recycling waste process. In that purpose, TiO_2 and composite made of TiO_2 and fly ash (FA) were synthetized and then characterized for their morphology, surface, structure and optical properties. The photo catalytic activity of TiO_2 and TiO_2-FA under solar irradiation was tested in the treatment of model solution containing an organic pollutant of choice; reactive azo dye C.I. Reactive Red 45 (RR45). Despite the current focus set on micro pollutants and contaminants of emerging concern [15,16], the colored waste waters still present rather serious environmental problem, not only from the aesthetic point of view. Namely, the production and application of dyes needed in vast array spheres of everyday life, increase continuously [17]. Among them, reactive azo dyes are most commonly used in textile industry due to their excellent applicative properties. However, they are characterized with a high hydrolization rate, yielding large dye content in dye bath effluents and eventually in waste streams of dye houses [18]. Such streams are documented to pose health hazards caused by non-biodegradable nature of present constituents, as well as their toxicity and potentially carcinogenic nature [19,20]. Thus, they need to be treated prior to discharge into the natural effluents. Accordingly, solution containing reactive dyes is quite representative case for testing a potential tertiary treatment option.

2. Experimental

2.1. Chemicals and materials

Following chemicals were used in the study without any further purification: hydrochloric acid (HCl, 37%, Kemika), acetic acid (HAc) ($C_2H_4O_2$, 99.8%, Kemika), ethanol (EtOH) (C_2H_5OH, 99.7%, Kemika), sulphuric acid (H_2SO_4, >96%, Kemika), sodium hydroxide (NaOH, p.a., Kemika), potassium nitrate (KNO_3, p.a., Kemika), potassium hydroxide (KOH, p.a., Kemika), nitric acid (HNO_3, ≥90%, Sigma Aldrich), tetra-n-butyl titanate (TBT) ($Ti(OC_4H_9)_4$, 99%, Acros Organics), and didecyl dimethyl ammonium chloride (DDAC) ($C_{22}H_{48}ClN$, 97%, Lonza Ltd). The reactive azo dye C.I. Reactive Red 45 (RR45) was used as a model organic pollutant in the study. Fly ash (FA0) was obtained from Plomin Power Plant, Croatia. All aqueous solutions were prepared with the ultra pure water from the Millipore Direct-Q3 UV (Merck, Germany) water purification system.

2.2. Synthesis of photo catalytic materials

Two photo catalytic materials were synthesized; TiO_2 and composite made of TiO_2 and fly ash (TiO_2-FA). The procedure for the synthesis of TiO_2 was as follows. Firstly, the solution A was prepared by mixing of TBT and EtOH in the volume ratio 1 : 1 (20 mL of each chemical was used). The solution was afterwards enriched with HAc (20 mL of 3 M), added drop wisely under vigorous stirring (250 rpm). The final solution was additionally stirred for another 15 min at room temperature. Solution B was obtained by mixing DDAC (2.1 mL), EtOH (60 mL) and H_2O (20 mL) distilled water; stirring took for 15 min at room temperature. Afterwards, the obtained solution B was added drop wisely into solution A and the resultant mixture was three times mixed for 15 min with high-speed disperser (7500 rpm) (T25 digital ULTRA-TURRAX, IKA, Germany). The mixture was then transferred in the Erlenmeyer flask, heated at 85°C in the laboratory oven (UN55, Memmert, Germany) for another 24 h until the transparent sol was obtained. The obtained precipitate, TiO_2, was washed for several times with distilled water, then dried at 100ºC for 12 h, and afterwards calcined in the laboratory furnace (LP-08, Instrumentaria, Croatia) at 400ºC for 3 h.

Prior the synthesis of TiO_2-FA, originally obtained FA samples (FA0) were treated with 3.5 M HCl, at elevated temperature in a water bath (95ºC) for 24 h and constant stirring (150 rpm), in order to increase its surface area by dissolving present $CaCO_3$ in its structure. According to the elemental analysis of FA0, performed by the supplier, the sample did not contain any traces of heavy metals. Such treated FA was coupled with TiO_2 to obtain TiO_2-FA composite using the procedure described above for TiO_2 synthesis; 16 wt% of FA was added into the solution A prior its coupling with solution B, while further steps remained the same as above.

2.3. Photo catalytic activity test

The experiments were performed in a water-jacket cooled batch reactor (V = 150 mL and T = 25.0 ± 0.2°C) using RR45 dye as a model organic pollutant (V_{RR45} = 100 mL) under simulated solar irradiation. As an irradiation source, 450 W Xenon arc lamp (Osram, Germany) situated in an appropriate lamp housing (Oriel/Newport, USA) with collimating optics, was used. An Oriel AM1.5 G air mass filter was situated in the path of the collimated beam, therefore mimicking the spectral characteristics of the solar spectrum when the Sun is at a zenith angle of 48.2º. The measured light intensity was 124.78 ± 0.11 mW cm^{-2}, determined using pyranometer CMP21 (Kipp & Zonen, Netherland). The intensity of UV-A fraction was determined to be 2.05 ± 0.07 mW cm^{-2}, using UVX radiometer equipped with UVX-36 longwave sensor (both UVP, UK). The concentration of RR45 in model solution was varied (10, 20, 30, 40, 80 and 100 mg L^{-1}), along with the process parameters: initial pH values (from 3 to 11) and dosages of photo catalyst used (TiO_2 or TiO_2-FA) (from 0.2 to 3.0 g L^{-1}) (Table 1). The later were varied through set matrix by used design of experiment (central composite design, CCD, Table 2). Adequate mixing of the solution was ensured using a magnetic stirrer (250 rpm). The experimental pro-

Table 1
Applied experimental range and the levels of independent variables used in studied solar photo catalytic treatment of RR45 dye using TiO_2 and TiO_2-FA

Process parameter	Coded value	Levels				
		–1	–0.5	0	0.5	1
pH	X1	3	5	7	9	11
γ(catalyst) (mg L^{-1})	X2	0.2	0.9	1.6	2.3	3.0

Table 2
Central composite design matrix with two independent variables expressed in coded units and actual value, and RR45 removal obtained by solar/TiO_2 and solar/TiO_2-FA during initial dark period and total

Exp #	Variables				Experimental results			
	Variable 1, X_1		Variable 2, X_2		Dark (ads)		Total	
					TiO_2	TiO_2-FA	TiO_2	TiO_2-FA
	Coded	pH	Coded	γ(catalyst) g L^{-1}	Removal, %			
1	–1	3	–1	0.2	2.85	3.52	5.21	10.31
2	1	11	–1	0.2	0.62	0.96	2.03	3.45
3	–1	3	1	3	31.92	25.91	81.75	81.38
4	1	11	1	3	2.22	0.85	10.72	9.89
5	0	7	1	3	12.12	7.69	41.82	29.56
6	1	11	0	1.6	2.14	2.13	7.90	5.80
7	0	7	–0.5	0.9	8.78	2.59	35.54	3.16
8	–1	3	0	1.6	17.64	14.16	58.17	37.04
9	–0.5	5	0.5	2.3	22.34	20.42	52.24	43.90
10	0.5	9	0.5	2.3	12.13	6.63	42.05	10.77
11	0	7	–1	0.2	2.15	2.13	4.13	2.60
12	–1	3	–1	0.2	2.90	3.42	4.86	9.80
13	1	11	–1	0.2	0.52	0.88	2.00	3.52
14	–1	3	1	3	32.13	26.41	82.05	82.62
15	1	11	1	3	2.13	0.98	9.97	9.55
16	1	11	0	1.6	2.21	2.23	8.07	6.13

cedure was following. (i) A desired concentration of RR45 solution was prepared by dissolving an adequate aliquot from "mother" solution (1 g L^{-1}) in water. (ii) The initial pH value of solution was adjusted at desired value (according to CCD used) by 1 M NaOH or H_2SO_4. (iii) The adequate amount of photo catalyst (TiO_2 or TiO_2-FA) requested to reach desired value according to CCD was then added into the reactor. (iv) The obtained suspension was stirred firstly in the dark for 30 min in order to ensure the adsorption/desorption equilibrium, and then was exposed to simulated solar irradiation for the requested period of treatment time. The duration of experiments varied according to their intention. The overall duration of experiments (including dark period and period under solar irradiation) was 90 min (the screening of influence of process parameters and RR45 concentration on the process effectiveness; 1st set), 210 min (experiments with prolonged treatment time; 2nd set) or 120 min (the testing of re-usability of studied photo catalysts; 3rd set). The samples were taken from the reactor in the predefined periods: –30, 0, 15, 30, 45, 60 for 1st set; –30, 0, 1, 3, 5, 10, 15, 20, 30, 45, 60, …195, 210 for 2nd set; and –30, 0, 30, 60, 90 for 3rd set, then filtered using Chromafil XTRA RC (25 mm, 0.45 μm, Macherey Nagel, Germany) and immediately submitted to analyses. All experiments in 1st and 3rd set were repeated three times, while experiments in the 2nd set were performed in octuplets by varying the sampling period between them in order to achieve respective results to calculate their average and not to spend more than 10% of reaction solution during experiment for the analytical purposes. The reproducibility of the experiments was >95.9%.

The studied photo catalysts TiO_2 and TiO_2-FA were tested for its reusability through three consecutive cycles, where experiments under identical conditions (3rd set) were performed. After each cycle the photo catalysts were recovered from the solution by decantation, submitted to drying

cycle at room temperature for 12 h, and afterwards were reused in the next cycle.

2.4. Analyses

The gas sorption analysis, performed using ASAP 2000 instrument (Micro meritics, USA), was used to determine the specific surface area and total pore volume of both original and treated fly ash (FA0 and FA). The samples were degassed at 400°C and subjected to N_2 adsorption. Brunauer–Emmett–Teller (BET) surface area was calculated from BET plot, while total pore volume was calculated using Barrett-Joyner-Halenda (BJH) model. The crystal phases in original (FA0) and as-prepared samples (FA, TiO_2 and TiO_2-FA) were identified by X-ray diffraction (XRD) using Shimadzu XRD6000 device (Japan) with CuKα radiation under accelerating voltage of 40 kV and current of 30 mA. Data were collected in 2θ range 5–70° in a step scan mode with steps of 0.02° and counting time of 0.6 s. Qualitative analysis was performed using X'Pert High Score Plus software. Diffuse reflectance spectra (DRS) of original (FA0) and as-prepared samples (FA, TiO_2 and TiO_2-FA) were measured over the range 200–800 nm at a spectral resolution of ~0.3–10 nm using USB 2000+ UV/Vis Spectrometer (Ocean Optics, USA). The acquired reflectance *vs.* wavelength spectra were transformed into the Kubelka–Munk function (KM) *vs.* photon energy ($h\nu$) in order to obtain the band gap values of primarily photo catalytic materials [21,22]. Microstructure and the morphology of the studied particles (FA0, FA, TiO_2 and TiO_2-FA) were analyzed using scanning electron microscope (SEM) Tescan Vega 3 (Czech Republic) at 20 kV. Before analyzes the samples were sputter coated with thin layer of Au/Pd.

Decolorization of RR45 model dye solution was monitored by UV/VIS spectrophotometer, Lambda EZ 201 (Perkin Elmer, USA), measuring the absorbance in visible spectra at characteristic wavelength of used RR45 dye (λ_{max} = 542 nm). The mineralization of RR45 dye solution was established on the basis of total organic carbon content measurements (TOC), performed by Total Organic Carbon analyzer; TOC-V_{CPN} (Shimadzu, Japan). Chemical (COD) and biochemical oxygen demand (BOD_5) were determined by colorimetric methods using HACH DR2800 spectrophotometer, and reagent kits LCK414 (for COD) and LCK554 (for BOD), all Hach-Lange, USA. Handylab pH/LF portable pH-meter (Schott Instruments GmbH, Germany) was used for adjusting pH prior photo catalytic treatment and for pH monitoring during potentiometric titration applied for the determination of point of zero charge (pH_{PZC}) values of synthetized materials (TiO_2 and TiO_2-FA). The pH_{PCZ} values were determined applying modified procedure of Uppal et al. [23]; detail description provided in our previous study [24].

2.5. Calculations

The influence of process parameters; initial pH values and dosages of photo catalyst used (TiO_2 or TiO_2-FA), on the effectiveness of solar photo catalytic treatment of RR45 dye solution was screened by means of response surface modeling (RSM). The values of aforementioned process parameters were transferred into the dimensionless coded values and represented by independent variables: X_1 and X_2 (Tables 1 and 2). The experimental space, covering the ranges of studied parameters and their combinations, was described using Central composite design (CCD) (Table 2). Two responses were chosen for each photo catalytic process (solar/TiO_2 and solar/TiO_2-FA); RR45 decolorization during initial dark period and after entire treatment period. In such manner, the adsorption ability and photo catalytic activity of studied photo catalysts (TiO_2 and TiO_2-FA) were evaluated. The combined influence of studied parameters on process performance is described by quadratic polynomial equation representing RSM models [25]. The fitting of RSM models was evaluated by coefficient of determination (R^2) and the analysis of variance (ANOVA), using STATISTICA 12.7 (Stat Soft & Dell, USA) and Design-Expert 10.0 (Stat Ease, USA). Because decolorization was chosen as a system response, the influence of RR45 concentration on the process effectiveness was evaluated using traditional "one-factor-at-a-time" approach.

3. Results and discussion

3.1. Characterization of fly ash and photo catalytic materials

The fly ash (FA0), obtained as a waste material from a power plant, had no traces of heavy metals but was characterized with a large content of $CaCO_3$ (Table S1, Supplementary material). Accordingly, FA0 was treated using HCl in order to modify its structural properties by dissolving $CaCO_3$ with the aim at increasing of adsorption capacity, providing potential improvements in its ability to serve as TiO_2 carrier. Hence, fly ash samples before (FA0) and after HCl treatment (FA) were characterized using nitrogen isothermal adsorption-desorption method in order to determine the surface area characteristics. The results are given in Fig. 1A and Table 3. As can be seen, the specific surface area (BET) and total pore volume of FA sample are approximately three times higher than that of FA0 (Table 3), indicating on rather significant removal of $CaCO_3$ by HCl treatment**.** The typical isotherm hysteresis for the porous systems can be seen for both FA0 and FA samples (Fig. 1A). It corresponds to nitrogen mono layer at relatively low pressure, and nitrogen multilayer at relatively higher pressures [26]. In the case of FA the adsorption isotherm and hysteresis loop significantly increased at lower relative pressures, indicating higher number of pores than in the case of FA0. The shape and position of the hysteresis of FA0 sample shows presence of very low fraction of pores, as can be observed from the value of the volume absorbed (Fig. 1A). Additionally, SEM analysis of FA0 and FA samples (Fig. 1B and C, respectively) revealed completely different morphology between them; the treated sample (FA) exhibits morphology with globules, while untreated (FA0) is less shape-defined.

Table 3
Specific surface area and total pore size of used fly ash samples

Samples	BET ($m^2\ g^{-1}$)	Total volume pore ($cm^3\ g^{-1}$)
FA0	3.9310	6.312×10^{-3}
FA	12.8021	16.120×10^{-3}

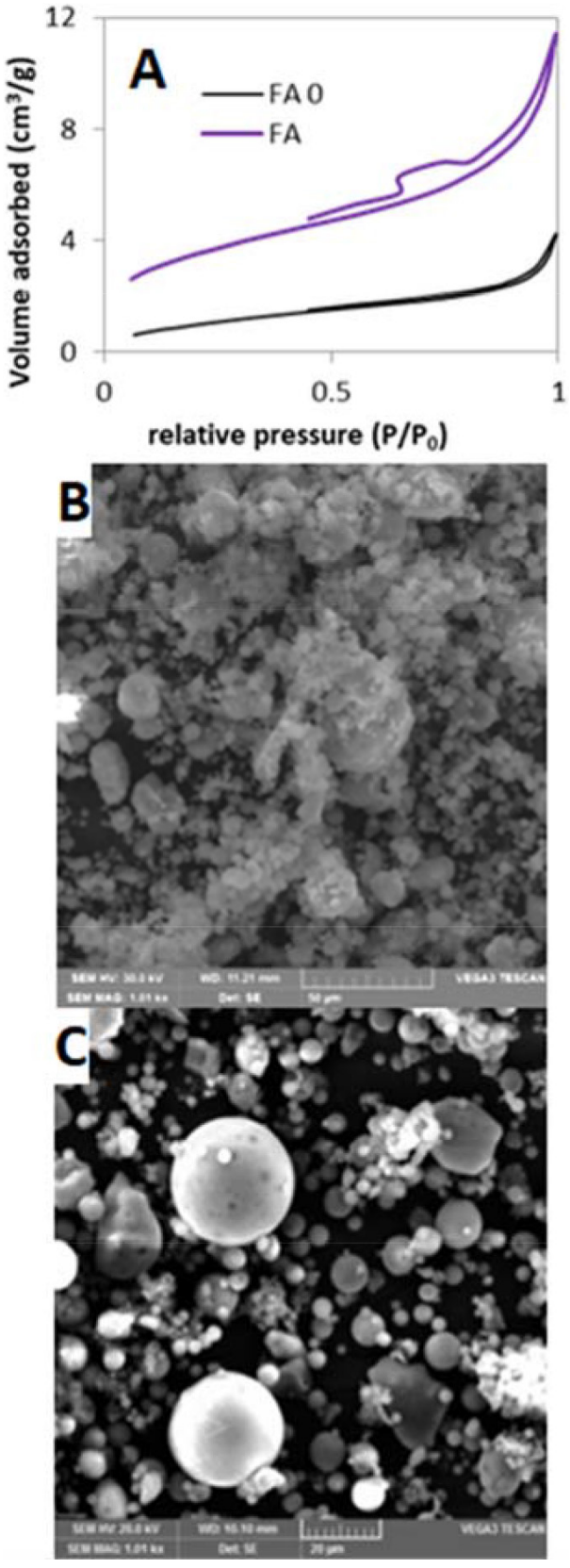

Fig. 1. Characterization of fly ash before (FA0) and after treatment (FA): nitrogen adsorption-desorption isotherms (A), SEM micro graphs of FA0 (B) and FA (C).

The both fly ash samples, along with synthetized photo catalysts (TiO_2 and TiO_2-FA) were characterized by XRD analysis (Fig. 2). Obtained diffractograms consist of narrow diffraction lines suggesting well-crystalline materials (Fig. 2A). FA0 yields crystalline phases: quartz (ICDD PDF#46-1045), mullite (ICDD PDF#79-1450), calcite (ICDD PDF#05-0586), calcium silicate (ICDD PDF#49-0442), hematite (ICDD PDF#33-0664) and magnetite (ICDD PDF#19-0629), all common in crystalline composition of fly ash [27]. The amorphous phase is also observed at broad hump centered at 23° 2θ, and most likely corresponds to amorphous silica, also common in fly ash composition. FA sample, corresponding to the treated fly ash, yields the same phases as FA0, with an important exception (Fig. 2A). The calcite fraction is completely leached out while the remaining crystal phases increased as a consequence of the modification process i.e. the dissolution of $CaCO_3$. It is worth of noting that the amorphous quantity in FA sample remains almost unchanged upon modification process using HCl (Fig. 2A). Taking into account the differences in morphology and crystallinity between FA0 and FA (Fig. 1B and C, Fig. 2A), one can conclude that less-defined morphology of FA0 is related to the presence of $CaCO_3$. Hence, calcite covered the surface of globules, thus decreasing the surface properties of the untreated material, FA0. In Fig. 2B the diffractograms of synthetized photo catalytic materials TiO_2 and TiO_2-FA are compared with that of AEROXIDE TiO_2 P25, a benchmark material. As can be clearly seen synthetized materials are characterized with peaks at 25.4° and 48.0°, confirming the presence of anatase structure within. On the other hand, their XRD patterns lack the peaks at 27.5°, 36.1° and 54.4°, typical for rutile phase, that are present in benchmark material TiO_2 P25 (Fig. 2B). Accordingly, the diffractograms of TiO_2 and TiO_2-FA exhibit anatase (ICDD PDF#21-1272) as the only crystalline phase related to TiO_2, while their broad shape indicates on the nano size of synthetized particles. In the composite sample, TiO_2-FA, the additional lines in diffractogram can be observed, pertaining to FA constituents with the highest content (i.e. strongest crystalline lines as observed in Fig. 2A); quartz (ICDD PDF#46-1045) and mullite (ICDD PDF#79-1450).

The UV/Vis reflectance spectra of studied materials are given Fig. 3; the shapes for TiO_2 and TiO_2-FA are very similar, while those corresponding to FA0 and FA show significant deviation in reflectance. Their reflectance started at 15% and did not change significantly in range from 200 to 320 nm, while it increased up to 32 and 38 % at 800 nm for FA and FA0, respectively. On the other hand, TiO_2 and TiO_2-FA show rather broad band; both samples are characterized with lower reflectance in the range of 220–380 nm, while in the visible spectra (380–800 nm) significantly higher reflectance with no maximum was observed. The light reflectance intensity indicates on the material photo activity in certain UV/Vis spectra range [28,29], while corresponding band gaps values provide more clear relationship. Hence, we transferred obtained reflectance using Kubelka–Munk function (K-M) and presented obtained results *vs.* photon energy ($h\nu$), (Fig. 3B). As can be seen, the plotted $F(R)^{1/2}$ *vs.* E_g exhibit flat sections only in the case of TiO_2 and TiO_2-FA, thus indirect band gap values are calculated only for them. The band gap of 3.05 eV was calculated for TiO_2, which is a similar value to corresponding materials of anatase struc-

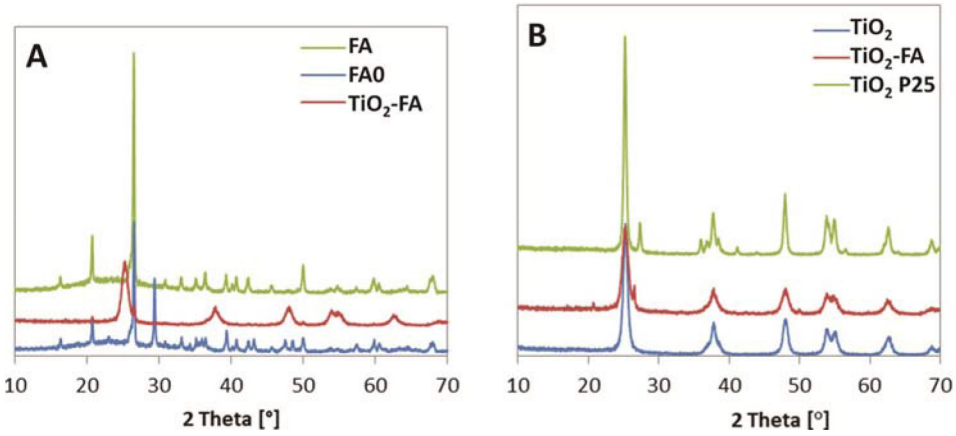

Fig. 2. X-ray diffraction patterns of studied materials: FA0, FA, and TiO_2-FA (A), and TiO_2, TiO_2-FA and AEROXIDE TiO_2 P25 (B).

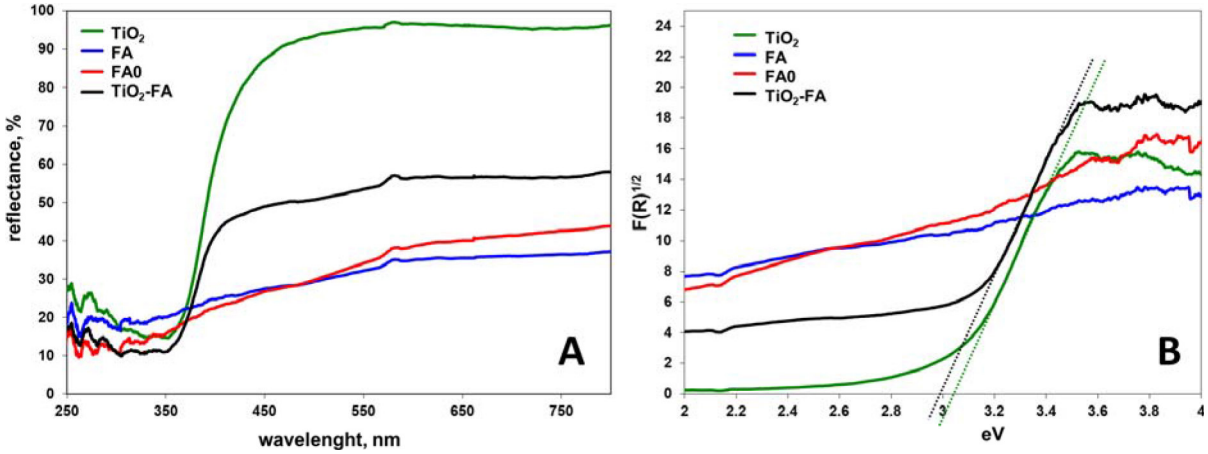

Fig. 3. Diffuse reflectance spectra of studied materials: FA, FA0, TiO_2, and TiO_2-FA (A), and corresponding plots of transformed Kubelka-Munk function vs. the energy of the light (B).

ture in the literature [21,24]. On the other hand, the composite showed slightly lower band gap value, 2.99 eV (Fig. 3B), indicating that TiO_2-FA might be more active under visible irradiation. In addition, the intensity of reflectance for the composite is between the reflectance for the pure components (TiO_2, FA), presumably due to its homogeneous composition as results of the established interactions between TiO_2 and FA (Fig. 3). The result of the SEM micro graphs, shown in Fig. 4, supports this assumption since the larger agglomerates of pure TiO_2 or FA has not been observed. On the contrary, the aggregation of pure TiO_2 has been reduced (as can be seen in Fig. 4a).

In Fig. 4 SEM micro graphs of synthetized species, TiO_2 and TiO_2-FA, are presented. As it can be seen from Fig. 4A, TiO_2 is present in smaller crystalline structures (Fig. 2B), as well as in bigger chucks, presumably agglomerated TiO_2 nanoparticles. On the other hand, in the case of TiO_2-FA composite (Fig. 4B), besides smaller structures, presumably TiO_2 not bonded into composite, globules structures, pertaining to FA, partially covered with TiO_2 crystallites can be observed (marked white circle). Accordingly, it can be concluded that composite structure is not quite uniform and consists of self-standing TiO_2 and TiO_2 deposited onto FA.

3.2. *Photo catalytic activity of studied materials*

The photo catalytic activity of synthetized TiO_2 and TiO_2-FA was studied under solar irradiation and on the model solution containing RR45 reactive azo dye. In the first step, the adsorption capacity of TiO_2 and TiO_2-FA in dark conditions toward RR45 dye, as well as susceptibility

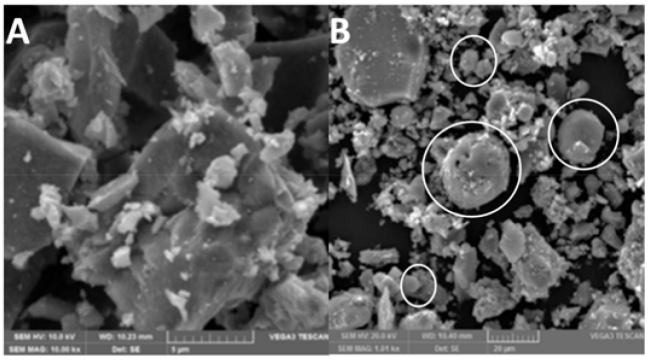

Fig. 4. SEM images of studied TiO_2 (A), and FA-TiO_2 (B).

of RR45 dye to be degraded directly under applied solar irradiation, were studied (Fig. S1, Supplementary material). The blank test related to the adsorption of RR45 in a dark is important due to the fact that reveals the adsorption of targeted pollutant onto used photo catalytic material. Additionally, it may provide an information on the appropriate dark period to establish adsorption/desorption before conducting the photo catalytic test under induced radiation. Namely, the adsorption is one of preconditions for effective photo catalytic degradation [2,3,30]. Hence, the blank test revealed two important effects; (i) the entire adsorption occurred in the first 30 min, and (ii) both materials exhibit similar adsorption of RR45 (17.3 and 14.5% by TiO_2 and TiO_2-FA, respectively) at studied conditions (pH 3 and 1.6 g L^{-1} of photo catalytic material). Accordingly, the initial dark period prior exposure to solar irradiation in duration of 30 min would ensure adsorption/desorption equilibrium between RR45 and studied photo catalytic materials. Another blank test performed, the direct photolytic RR45 degradation under solar irradiation, is important in order to distinguish the photo catalytic and photolytic effects occurring in the overall degradation of targeted pollutant. According to obtained results, it can be concluded that RR45 degradation under solar irradiation is rather limited in the absence of any photo catalytic material; after 90 min treatment a rather negligible decolorization extent of RR45 dye solution, 0.3%, was achieved (Fig. S1, Supplementary material).

Taking into account the findings from performed blank tests, the photo catalytic activity of studied materials toward RR45 dye is performed varying the process parameters: pH and dosage of photo catalyst (experimental matrix set by CCD, Table 2), as well as initial RR45 concentration. In Fig. 5 a comparison of RR45 removals using TiO_2 and TiO_2-FA under solar irradiation at conditions set by CCD is presented (Table 2). As can be seen, a noticeable RR45 removal after entire photo catalytic treatment (>80%) is achieved only in experiments #3 and #14 (Fig. 5), which are actually replicates performed at pH 3 and with 3 g L^{-1} of photo catalysts. Interestingly, the overall effectiveness of processes conducted with TiO_2 and TiO_2-FA did not differ, in spite of slightly better adsorption results in initial dark period achieved with TiO_2; for 6% better RR45 removal in comparison to the case using TiO_2-FA (exps. #3 and #14, Fig. 5, Table 2). In all other conditions studied, process using TiO_2 showed better or remarkably better (e.g. exps. #5, #7, #8, #9 and #10, Fig. 5) overall effectiveness comparing to that using composite. The exceptions are cases with rather poor RR45 removal; lower that 10% in overall (exps. #1, #2, #12, and #13, Fig. 5). Since no clear pattern in behavior of both processes was observed through given presentation, the obtained RR45 removals, both after initial dark period and overall, were modeled using RSM.

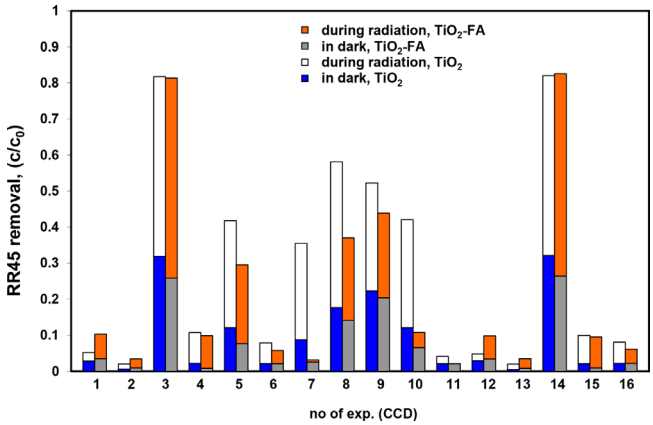

Fig. 5. Comparison of RR45 removal using TiO_2 and TiO_2-FA under solar irradiation at conditions set by CCD (Tables 1 and 2).

Using this approach one may get insight in the influence of the process parameters of the photo catalytic treatment avoiding the misleading information that might be obtained using "one-parameter-at-the-time" approach [2,31]. The first postulate for such action is to have accurate, significant and predictive models. Most commonly, the evaluation of RSM models is based on statistical parameters, either numerical obtained from analysis of variance (ANOVA): Fisher *F*-test value (*F*), its probability value (*p*), regression coefficients (pure; R^2, adjusted; R_{adj}^2, predicted; R_{pre}^2), *t*-test value, or graphical based on so-called "residual diagnostic" (RD): normal probability test, Levene's test, and constant variance test [25,32–34]. Hence, the multiple regression analysis was applied on CCD matrix and RR45 removal extents obtained after initial dark period and overall photo catalytic treatment i.e. system responses (Table 2), yielding polynomial equations given in Table S2 (Supplementary material). Afterwards, such obtained models M1–M4 are characterized by ANOVA (Tables S3 and S4, Supplementary material) and RD (example is given in Fig. S2, Supplementary material). Basically, all models were found to be significant (all having $p < 0.0001$), and accurate ($0.961 < R^2 < 0.989$ and $0.941 < R_{adj}^2 < 0.984$), while RD revealed that (i) there are no violations in the assumptions that errors are normally distributed and independent of each other, (ii) the error variances are homogeneous, and (iii) residuals are independent. Accordingly, these M1–M4 models can be used hereinafter as a tool to enlighten the influence of studied parameters (initial pH and photo catalyst dosage) on RR45 adsorption and solar driven photo catalytic treatment using TiO_2 and TiO_2-FA.

Fig. 6 shows 3D surface and contour presentations of the influence of initial pH and photo catalyst dosage on RR45 removal after initial period and overall solar photo catalytic treatment using TiO_2 and TiO_2-FA modeled by M1, M2, M3 and M4, respectively. Although 3D surfaces for dark adsorption are rather similar (Fig. 6A and 6C), several differences can be noticed. Regardless the photo catalyst applied, adsorptive removal of RR45 is fairly limited at basic conditions, but is promoted at acidic conditions, especially at higher dosages of applied photo catalysts. However, somewhat higher RR45 removal extents were achieved with TiO_2 at comparable conditions. Similar results were also obtained during blank tests (Fig. S1, Supplementary material). Such results can be assigned to the higher overall adsorptive capacity of TiO_2 over TiO_2-FA, presumably due to differences in surface area and pH_{PZC} values (Fig. S3, Supplementary material). Namely, it was established that pH_{PZC} value of TiO_2 is higher than that of TiO_2-FA; 6.62 > 4.41. It should be noted that determined pH_{PZC} value of TiO_2 is in accordance with literature findings [24,35]. The obtained pH_{PZC} value for the composite TiO_2-FA can be associated

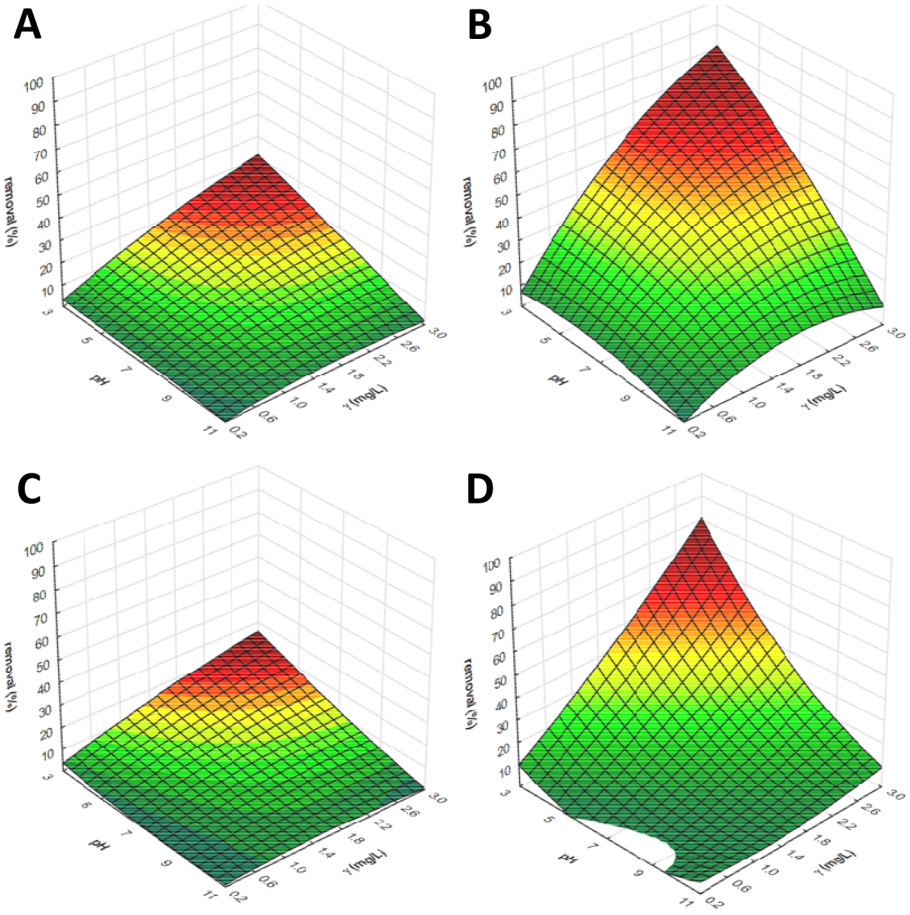

Fig. 6. 3D response surface and contour diagrams showing the effects of the mutual interactions of initial pH and γ(catalyst) on the RR45 obtained by solar/TiO_2 during initial dark period (A) and total (B) and by solar/TiO2-FA during initial dark period (C) and total (D).

with the remained acidic content during FA treatment. The 3D surface plots representing the influence of initial pH and photo catalyst dosage on the overall photo catalytic effectiveness, although sharing maximum area (lowest pH and highest photo catalyst dosage), are of completely different shape. The one corresponding to solar/TiO_2 process (Fig. 6B) has concave shape, while the other corresponding to solar/TiO_2-FA process is of convex shape (Fig. 6D). Usually concave shape, observed for solar/TiO_2 process (Fig. 6B), can be assigned to the saturation effect, i.e. too high dosage of photo catalytic particles in the system, yielding increased recombination of photo generated electron-hole (e^-/h^+) pairs and photon-shielding effect due to decreased transparency, both lowering the process effectiveness [2,3,36]. If we consider that photon-shielding effect would take place in solar/TiO_2-FA process as well (although in smaller extent due to larger and heavier FA particles), the convex shape observed here can be assigned to the fact that TiO_2 content was not the same at the same weight of added photo catalyst. TiO_2-FA had 16 wt.% of non-photo catalytically active particle (FA), and most likely the increased recombination of formed e^-/h^+ pairs was not reached in the studied range. Thus, the process effectiveness remarkably increased by increasing TiO_2-FA dosage (Fig. 6D). Common effects observed in photo catalytic treatment using TiO_2 and TiO_2-FA are similar to those observed in dark adsorption; limited RR45 removal at basic conditions and significant improvements in processes effectiveness by decreasing pH and increasing photo catalyst dosage (Fig. 6.). According to the photo catalysis mechanism, the precursors for hydroxyl radicals ($HO^\bullet$) and super oxide radicals ($O_2^{-\bullet}$) formed at photo generated h^+ and e^- upon the excitation of photo catalytic material by the sufficient energy, are HO^- and (dissolved) O_2 [1,2]. In theory $HO^\bullet$ formation, as the main reactive specie in the non-aerated system (as ours), would be higher at elevated pH (due to higher concentration of HO^-) [1–3]. Thus, one may conclude that process effectiveness would be higher at basic conditions. However, our results clearly support the above-stated importance of adsorption within photo catalytic degradation mechanism. Namely, the effective adsorption on the catalyst surface precedes effective degradation of organics by photo catalytic treatment. In such case, the degradation occurs at the surface directly on photo generated h^+ or indirectly by formed reactive oxygenated species (ROS, predominately $HO^\bullet$ and $O_2^{\bullet-}$), overcoming mass transfer limitations related to their diffusion into the solution [2,37]. The increase in process effectiveness by increasing the photo catalyst dosage is logical; (i) more photo catalytic material means more active places where h^+ and e^- can be generated, and (ii) higher sur-

face area for adsorption of targeted organic pollutant [2,38]. However, the negative influence of too high dosage related to saturation effect should be considered as well. Actually, that effect was in part reflected in the case of TiO_2, resulting with the concave shape of 3D surface (Fig. 6B).

The results obtained within testing the influence of initial RR45 concentration on the effectiveness of solar/TiO_2 and solar/TiO_2-FA processes are presented in Fig. 7 (comparison of studied processes for each initial RR45 concentration) and Fig. S4 (Supplementary material) (comparison of studied initial RR45 concentrations for each process). Three common effects can be seen from Fig. 7. (i) When absolute values are considered, RR45 removal during dark period is the same regarding the same particle type; ~3.5 and ~3.2 mg are removed by 1.6 g L^{-1} of TiO_2 and TiO_2-FA, respectively. (ii) Regardless the catalyst type and initial RR45 concentrations, RR45 removals achieved after exposure to solar irradiation obeyed first-order kinetics, which is in accordance with the literature [3,39]. (iii) Solar/TiO_2 process showed higher effectiveness at all studied RR45 concentrations comparing to the process with TiO_2-FA. Although in some cases the differences seem to be large (between 10 and 15%) (Fig. 6(A) and 6(B)), when absolute values are compared the difference in effectiveness is almost similar

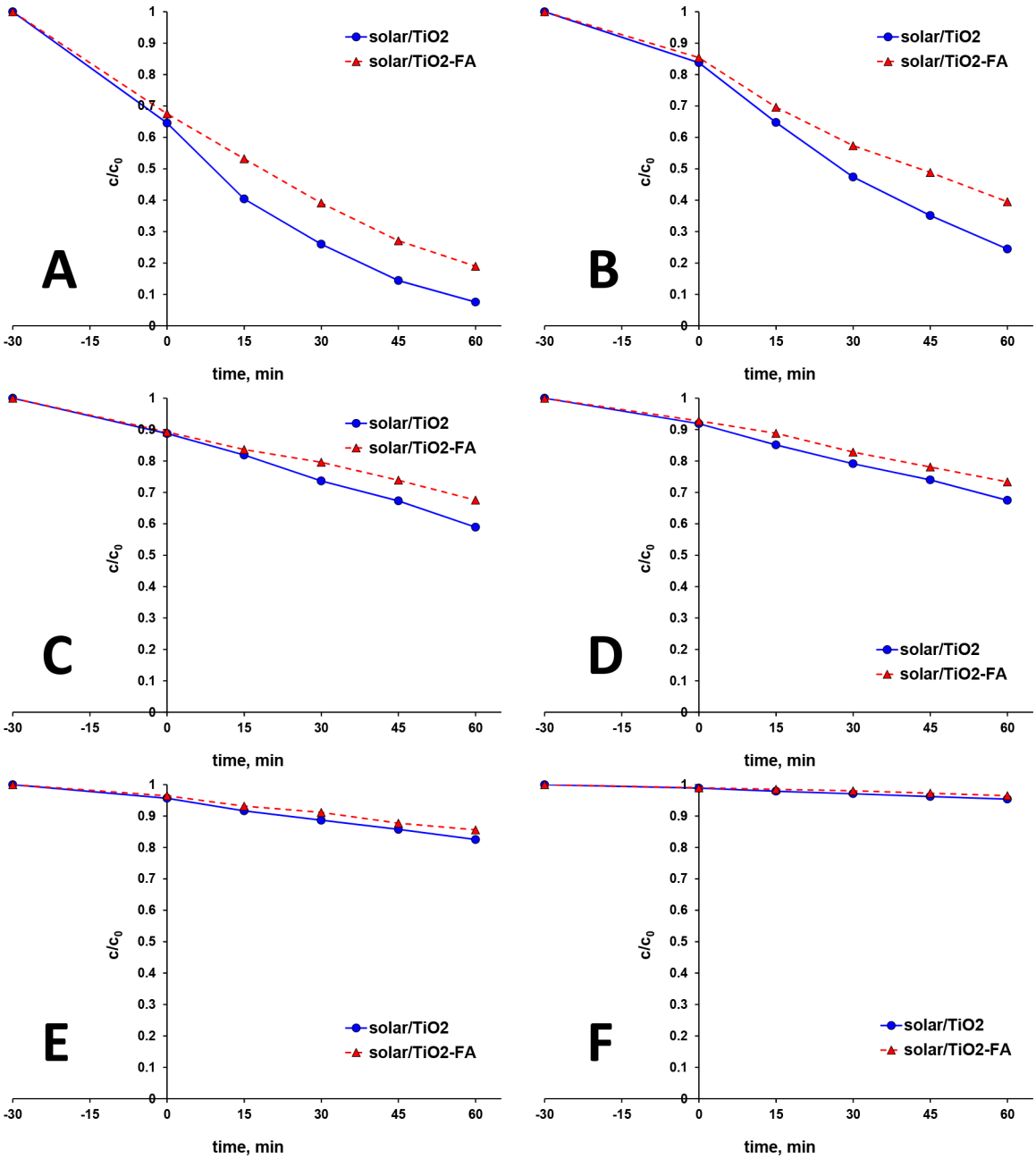

Fig. 7. The influence of initial RR45 concentration on the effectiveness of solar/TiO_2 and solar/TiO_2-FA: 10 mg L^{-1} (A), 20 mg L^{-1} (B), 30 mg L^{-1} (C), 40 mg L^{-1} (D), 80 mg L^{-1} (E), and 100 mg L^{-1} (F) (pH 4.8, $\gamma(TiO_2)$ = 1.6 g L^{-1}, $\gamma(TiO_2\text{-FA})$ = 1.6 g L^{-1})

regardless the initial RR45 concentration; ~2.8 mg of RR45 remained non-degraded by solar/TiO_2-FA process. This result speaks in favor to the above-mentioned lack of photo catalytic material in the case of TiO_2-FA when comparing the processes with dosages of TiO_2 or TiO_2-FA. Considering the relative RR45 removal efficiency, as presented in Fig. 7, one can conclude that process effectiveness decreases with the increase of initial RR45 concentration. However, when observing absolute values the effect is not straightforward. For example, when the concentration of dye increased from 10 to 20 mg L^{-1}, the process effectiveness also increased; from 9.2 to 14.5 mg and from 8.1 to 12.1 mg degraded by solar/TiO_2 and solar/TiO_2-FA, respectively (Figs. 7(A) and (B), and S4, Supplementary material). The further increase in initial dye concentration up to 30, 40 and even 80 mg L^{-1} resulted in somewhat lower process effectiveness; ~12.5 and ~10.5 mg of RR45 were degraded by solar/TiO_2 and solar/TiO_2-FA, respectively (Figs. 7(C), (D) and (E), and S4, Supplementary material). When initial RR45 concentration increased at 100 mg L^{-1} the significant drop in process effectiveness was observed; less than 5 mg of RR45 was degraded in both studied processes (Figs. 7F and S4, Supplementary material). Taking into account that (i) same conditions (initial pH and photo catalyst dosage) were applied, (ii) similar RR45 removals during initial dark period were achieved (in absolute values), and (iii) photo-shielding effect occurred as a consequence of increased initial RR45 concentration, such behavior can be explained with the fact that most probably organic radical species were formed during partial RR45 degradation. Hence, more RR45 molecules present in the system, more organic radicals were formed and involved in further RR45 degradation. Similar effects were reported in the literature [40,41]. However, it seems that such positive effect was overcame by non-transparent nature of reaction solution when RR45 concentration increased to 100 mg L^{-1}, resulting in rather poor effectiveness of solar driven photo catalytic process (Figs. 7 and S4, Supplementary material).

In the next test, the influence of treatment time on the effectiveness of studied solar driven photo catalytic processes using TiO_2 and TiO_2-FA was investigated. The results obtained during prolonged treatment, i.e. upon achieving the complete RR45 removal, with at least one process, are presented in Fig. 8. An interesting effect can be observed during initial period of treatment under solar irradiation; rather similar RR45 removal extents were recorded regardless the catalyst applied. The discrepancies in process effectiveness started to be more evident after 15 min treatment and were enlarged with the treatment time prolongation. The obtained results are most likely the consequence of different content of photo catalytically active material in spite of the same overall weight of photo catalysts. According to here obtained results, the mineralization effectiveness was compared. The mineralization of RR45 dye solution was determined at the same decolorization extents (Fig. 9). As can be seen, when 25% decolorization of RR45 solution was achieved, rather low amount of organic content was mineralized; <1% in both processes. By progressing of RR45 degradation, i.e. by increasing the decolorization extent up to 50% and 75%, more significant mineralization extents were recorded; 14.5 and 25.0 % by solar/TiO_2 and 11.7 and 21.0 % by solar/TiO_2-FA. Finally, a remarkable amount of organic content was mineralized after achieving almost complete decolorization of RR45 solution; 52.3 and 37.9 % by solar/TiO_2 and solar/TiO_2-FA, respectively (Fig. 9.). Taking into account the degradation mechanism of dyes with similar structure [40,41], one can conclude that chromophoric group of RR45, responsible for the coloration of solution, is the weakest part of dye molecule and was firstly attacked by ROS. Hence, decolorization in higher extent must precede the mineralization. Observing the differences in mineralization effectiveness regarding the photo catalyst type applied, one can conclude that mineralization is more promoted when TiO_2 was used. The reason for such behavior may be found in the fact that more active places at catalyst surface existed when only TiO_2 was present in the system. However, the determined biodegradability of RR45 dye solution at 90% decolorization showed similar results for both processes. Namely, BOD_5/COD values were improved significantly comparing to the initial value of untreated RR45 solution; from 0.05 (characterizing highly non-biodegradable water) to 0.42 and 0.41 (over biodegradability limits [42]) in the cases of solar/TiO_2 and solar/TiO_2-FA, respectively. These results indicate that degradation path-

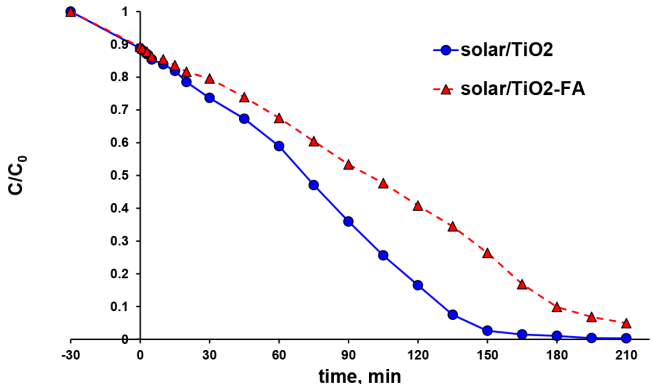

Fig. 8. The influence of treatment time on the effectiveness of solar/TiO_2 and solar/TiO_2-FA (pH 4.8, γ(RR45) = 30 mg L^{-1}, γ(TiO_2) = 1.6 g L^{-1}, γ(TiO_2-FA) = 1.6 g L^{-1}).

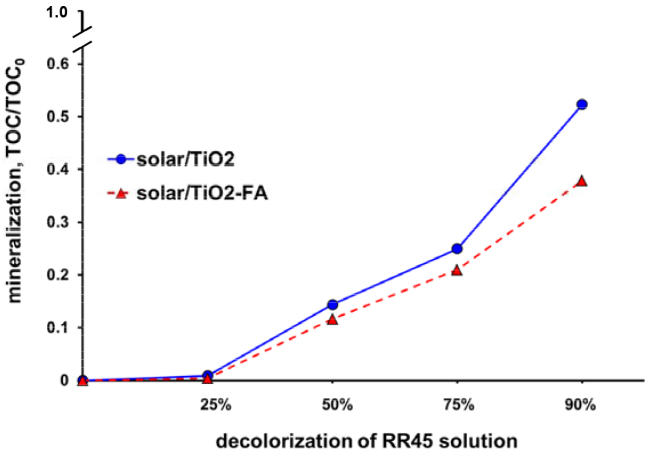

Fig. 9. Mineralization of RR45 dye solution regarding the decolorization percentage achieved by solar/TiO_2 and solar/TiO_2-FA (pH 4.8, γ(RR45) = 30 mg L^{-1}, γ(TiO_2) = 1.6 g L^{-1}, γ(TiO_2-FA) = 1.6 g L^{-1}).

ways occurring in performed solar driven photo catalytic treatments might be different; in spite of rather high discrepancy in mineralization achieved at 90% decolorization, similar biodegradability was obtained.

The final performed test within the study was a reuse of TiO_2 and TiO_2-FA through consecutive cycles (Fig. 10). As can be seen, the photo catalyst reuse resulted in the decreased effectiveness of both (i) adsorption during dark period and (ii) overall photo catalytic treatment, regardless the photo catalyst type. Hence, the adsorption capacity of TiO_2 in dark period lowered for ~4.5% in each consecutive cycle (Fig. 10A). Similar drop in adsorption effectiveness was recorded in the case TiO_2-FA, resulting with almost negligible adsorption during dark period of 3rd cycle (Fig. 10B). Similarly, overall effectiveness of photo catalytic treatments decreased between 7 and 10% through the cycles. Even higher drop in process effectiveness can be seen for achieved mineralization through the consecutive cycles (Fig. 10C). This effect can be assigned to the organic content remained at the catalyst surface from previous run, and in such manner (i) lowering the surface area and (ii) blocking the active sites for the formation of ROS [44]. Both effects would have negative influence on process effectiveness in reuse cycles. The organic content can be either RR45 dye molecules or formed by-products during RR45 degradation, adsorbed at the catalyst surface during the treatment process due to altered adsorption/desorption equilibrium. Similar effects were observed in our previous study [9]. Although easy to handle and maintain, the simple reuse of studied photo catalysts is not a favorable option, thus the reactivation of studied photo catalysts using either washing (water or bases) or more advanced techniques (thermal, UV, ozone, etc) [43–47] should be used to retain activity in the consecutive cycles.

Based on the above presented results, the set hypothesis of using FA as potential co-catalyst promoting overall composite photo activity under solar irradiation has not been confirmed. In spite of slightly lower band gap value, composite material had 16% lower content of sole photo catalytically active material (TiO_2), which caused lower effectiveness of process using composite. The other hypothesis; the use of FA, a waste material from power plant, as a carrier for TiO_2 in water treatment process, is partially confirmed by (i) morphology inspection, as well as (ii) reuse tests, where the separation of TiO_2-FA was much easier than that of sole TiO_2; the latter formed much thicker suspensions.

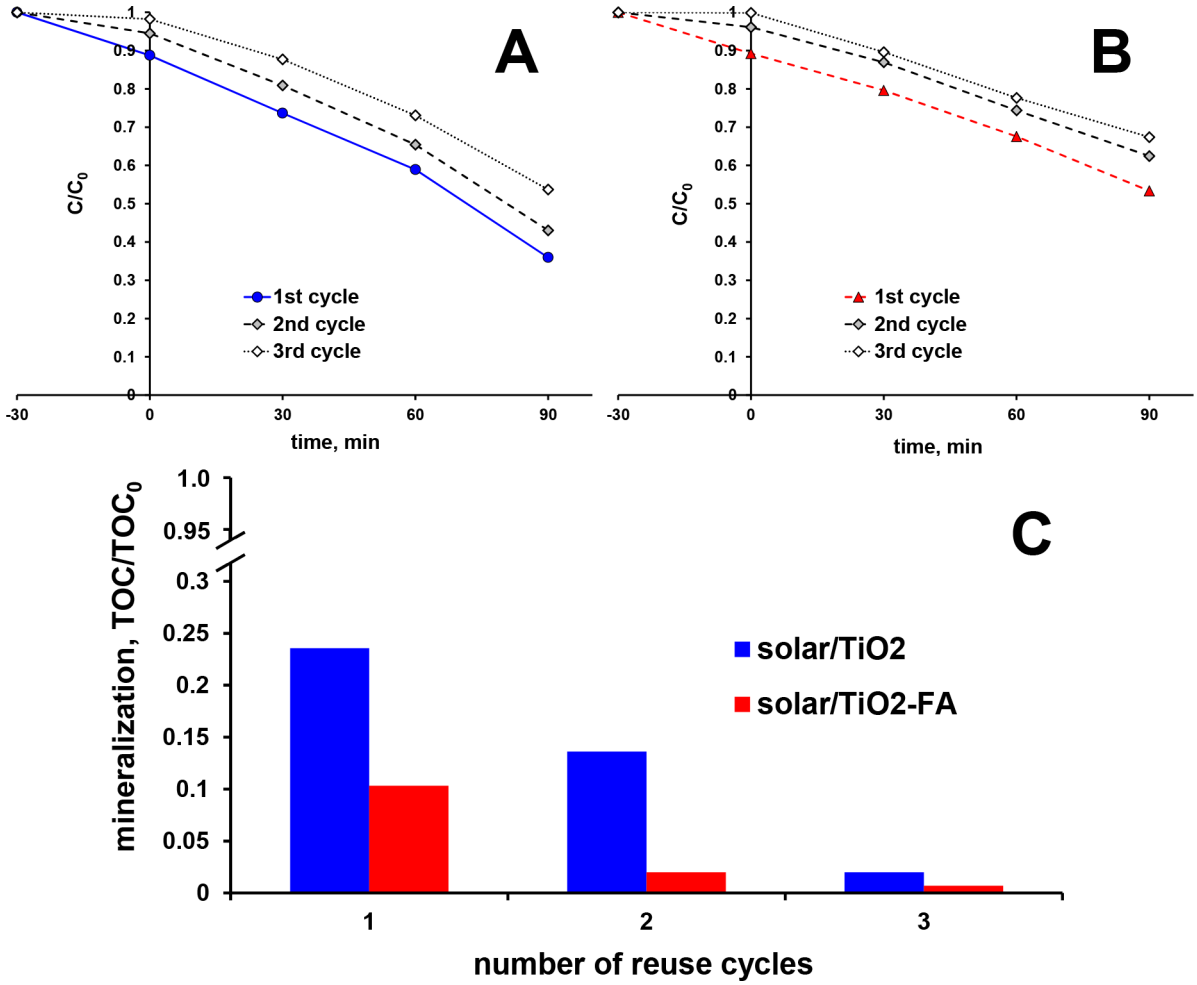

Fig. 10. Catalyst reuse study; effectiveness of solar/TiO_2 and solar/TiO_2-FA in RR45 solution decolorization and mineralization through 3 consecutive cycle (pH 4.8, γ(RR45) = 30 mg L^{-1}, γ(TiO_2) = 1.6 g L^{-1}, γ(TiO_2-FA) = 1.6 g L^{-1}).

4. Conclusions

The results of characterization of modified fly ash (FA) revealed the increased surface area due to removal of $CaCO_3$, confirmed by XRD and SEM analysis; complete leaching of calcite and clear spherical shapes were observed. Thus, the modification of fly ash successfully enhanced its property for the intended use as the TiO_2 catalyst carrier. The results from XRD analysis showed that synthetized TiO_2 is consistent of only anatase crystalline phase. The results of DRS analysis and corresponding Kubelka-Munk plots showed that modified fly ash contributed to the lower band gap of TiO_2-FA composite comparing to pure TiO_2, indicating that its photo activity under visible irradiation might also increase. SEM analysis revealed that TiO_2-FA composite does not have uniform composition but is consistent of self-standing TiO_2 and TiO_2 deposited onto FA.

The both studied photo catalysts TiO_2 and TiO_2-FA showed similar adsorption capacity throughout studied range of pH and applied dosages; TiO_2 exhibited slightly better RR45 removal during dark periods, presumably as consequence of its surface properties. Influence of studied processes parameters (initial pH, photo catalyst dosage and initial RR45 concentration) on RR45 degradation efficiency using TiO_2 and TiO_2-FA under solar irradiation was also similar. It was established that RR45 removal increased by decreasing the initial pH and increasing the photo catalyst dosage, mirroring the adsorption efficiency during initial dark period. Additionally, RR45 removal (in absolute values) was quite stable regardless of initial concentration (up to 80 mg L-1), indicating the involvement of organic radical species in the RR45 degradation. However, throughout studied range of process parameters, except the optimal area mentioned above (highly acidic pH and the highest photo catalyst dosage applied), process using TiO_2 showed better results than that using TiO_2-FA. Such effect can be assigned to the fact that composite had 16 wt% less photo catalytically active component (TiO_2). However, composite underwent easier separation after the treatment, but again, exhibited lower effectiveness then reused TiO_2.

Acknowledgement

We acknowledge the financial support from Croatian Science Foundation (Project IP-11-2013-5092; Development of Photo catalytic Polymer Nanocomposites for Wastewater Treatment (DePoN Photo)).

References

[1] J. Schneider, M. Matsuoka, M. Takeuchi, J. Zhang, Y. Horiuchi, M. Anpo, D.W. Bahnemann, Understanding TiO_2 photo catalysis: mechanisms and materials. Chem. Rev., 114 (2014) 9919–9986.

[2] P. Pichat, Photo catalysis and water purification: from Fundamentals to Recent Applications, Wiley, Germany, 2013.

[3] M.N. Chong, B. Jin, C.W.K. Chow, C. Saint, Recent developments in photo catalytic water treatment technology: a review, Water Res., 44 (2010) 2997–3027.

[4] M. Pelaez, N.T. Nolan, S.C. Pillai, M.K. Seery, P. Falaras, A.G. Kontos, P.S.M. Dunlop, J.W.J. Hamilton, J.A. Byrne, K. O'Shea, M.H. Entezari, D.D. Dionysiou, A review on the visible light active titanium dioxide photo catalysts for environmental applications, Appl. Catal., B 125 (2012) 331–349.

[5] R. Fagan, D.E. McCormack, D.D. Dionysiou, S.C. Pillai A review of solar and visible light active TiO_2 photo catalysis for treating bacteria, cyanotoxins and contaminants of emerging concern, Mat. Sci. Semicon. Proc., 42 (2016) 2–14.

[6] S. Mozia, P. Brozek, J. Przepiorski, B. Tryba, A.W. Morawski, Immobilized TiO_2 for phenol degradation in a pilot-scale photo catalytic reactor, J. Nanomater., 2012 (2012) 1–10.

[7] K. Naeem, F. Ouyang, Influence of supports on photo catalytic degradation of phenol and 4-chlorophenol in aqueous suspensions of titanium dioxide, J. Environ. Sci., 25 (2013) 399–404.

[8] F. Li, S. Sun, Y. Jiang, M. Xia, M. Sun, B. Xue, Photo degradation of an azo dye using immobilized nanoparticles of TiO_2 supported by natural porous mineral, J. Hazard. Mater., 152 (2008) 1037–1044.

[9] S. Salaeh, D.J. Perisic, M. Biosic, H. Kusic, S. Babic, U. Lavrencic Stangar, D.D. Dionysiou, A. Loncaric Bozic, Diclofenac removal by solar assisted photo calaysis using TiO_2-based zeolite catalyst; mechanisms, pathways and environmental aspects, Chem. Eng. J., 304 (2016) 289–302.

[10] P. Lei, F. Wang, X. Gao, Y. Ding, S. Zhang, J. Zhao, S. Liu, M. Yang, Immobilization of TiO_2 nanoparticles in polymeric substrates by chemical bonding for multi-cycle photo degradation of organic pollutants, J. Hazard. Mater., 227–228 (2012) 185–194.

[11] S. Liu, J. Zhu, Q. Yang, P. Xu, J. Ge, X. Guo, Preparation of SnO_2–TiO_2/fly ash cenospheres and its application in phenol degradation, Photochem. Photobiol., 91 (2015) 1302–1308.

[12] Y.T. Yu, Synthesis of nanocrystalline TiO_2-coated coal fly ash for photo catalyst, Korean J. Chem. Eng., 20 (2003) 850–854.

[13] M.R. Senapati, Fly ash from thermal power plants – waste management and overview, Current Sci., 100 (2011) 1791–1794.

[14] EC, Implementation of the Circular Economy Action Plan-http://ec.europa.eu/environment/circular-economy/index_en.htm (accessed on March 5, 2018).

[15] EU, Directive 2013/39/EU of the European Parliament and of the Council amending Directives 2000/60/EC and 2008/105/EC as regards priority substances in the field of water policy, Off. J. Eur. Commun., 226 (2013) 1–17.

[16] JCR Technical Report, Development of the First Watch List under the Environmental Quality Standards Directive. https://ec.europa.eu/jrc/en/publication/eur-scientific-and-technical-research-reports/development-first-watch-list-under-environmental-quality-standards-directive (accessed on Dec 20, 2017).

[17] D. Bhatia, N.R. Sharma, J. Singh, R.S. Kanwar, Biological methods for textile dye removal from wastewater: A review, Crit. Rev. Environ. Sci. Technol., 47 (2017) 1836–1876.

[18] K. Hunger, Industrial Dyes; Chemistry, Properties, Application, Wiley-VCH, Weinheim, Germany, 2002.

[19] H. Kusic, N. Koprivanac, A. Loncaric Bozic, Environmental aspects on the photo degradation of reactive triazine dyes in aqueous media, J. Photochem. Photobiol., A 252 (2013) 131–144.

[20] Y. Verma, Acute toxicity assessment of textile dyes and textile and dye industrial effluents using Daphnia magna bioassay, Toxicol. Ind. Health, 24(7) (2008) 491–500.

[21] R. Lopez, R. Gomez, Band-gap energy estimation from diffuse reflectance measurements on sol–gel and commercial TiO_2: a comparative study, J. Sol-Gel Sci. Technol., 61 (2012) 1–7.

[22] K. Koci, L. Obalova, L. Matejova, D. Placha, Z. Lacny, J. Jirkovsky, O. Solcova, Effect of TiO_2 particle size on the photo catalytic reduction of CO_2, Appl. Catal., B 89 (2009) 494–502.

[23] H. Uppal, J. Hemlata, N. Tawale, Singh Zinc peroxide functionalized synthetic graphite: An economical and efficient adsorbent for adsorption of arsenic (III) and (V), J. Environ. Chem. Eng., 4 (2016) 2964–2975.

[24] M. Kovacic, H. Kusic, M. Fanetti, U.L. Stangar, M. Valant, D.D. Dionysiou, A.L. Bozic, TiO_2-SnS_2 nanocomposites; solar active photo catalytic materials for water treatment, Environ. Sci. Poll. Res., 24 (2017) 19965–19979.

[25] R.H. Myers, D.C. Montgomery, C.M. Anderson-Cook, Response surface methodology: process and product optimization using designed experiments, 3rd ed., John Wiley & Sons, Hoboken, USA, 2009.

[26] Z. Sarbak. M. Kramer-Wachowiak, Porous structure of waste fly ashes and their chemical modification, Powder Technol., 123 (2002) 53–58.
[27] A. Duta, M. Visa, Simultaneous removal of two industrial dyes by adsorption and photo catalysis on a fly-ash-TiO_2 composite, J. Photochem. Photobiol. A., 306 (2015) 21–30.
[28] X. Chen, S.S. Mao, Titanium dioxide nanomaterials: synthesis, properties, modifications, and applications, Chem. Rev., 107 (2007) 2891–2959.
[29] D. Yang, H. Li, Z. Zheng, Y. Yuan, J. Zhao, E.R. Waclawik, X. Ke, H. Zhu, An efficient photo catalyst structure: TiO_2(B) nanofibers with a shell of anatase nanocrystals, J. Am. Chem. Soc., 131 (2009) 17885–17893.
[30] C. Zhao, M. Pelaez, D. Dionysiou, S.C. Pillai, J.A. Byrne, K.E. O'Shea, UV and visible light activated TiO_2 photo catalysis of 6-hydroxymethyl uracil, a model compound for the potent cyanotoxin cylindrospermopsin, Catal. Today, 224 (2014) 70–76.
[31] M. Kovacic, S. Salaeh, H. Kusic, A. Suligoj, M. Kete, M. Fanetti, U.L. Stangar, D.D. Dionysiou, A.L. Bozic, Solar-driven photo catalytic treatment of diclofenac using immobilized TiO_2-based zeolite composites, Environ. Sci. Poll. Res., 23 (2016) 17982–17994.
[32] K. Yetilmezsoy, S. Demirel, R.J. Vanderbei, Response surface modeling of Pb(II) removal from aqueous solution by Pistacia vera L.: Box-Behnken experimental design, J. Hazard. Mater., 171 (2009) 551–562.
[33] S. Debnath, N. Ballav, H. Nyoni, A. Maity, K. Pillay, Optimization and mechanism elucidation of the catalytic photo-degradation of the dyes Eosin Yellow (EY) and Naphthol blue black (NBB) by a polyaniline-coated titanium dioxide nanocomposite, Appl. Catal. B., 163 (2015) 330–342.
[34] M. Dopar, H. Kusic, N. Koprivanac, Treatment of simulated industrial wastewater by photo-Fenton process: Part I. The optimization of process parameters using design of experiments (DOE), Chem. Eng. J., 173(2) (2011) 267–279.
[35] N.T. Boncagni, J.M. Otaegui, E. Warner, T. Curran, J. Ren, M. M. Fidalgo de Cortalezzi, Exchange of TiO_2 nanoparticles between streams and stream beds, Environ. Sci. Technol., 43 (2009) 7699–7705.
[36] D.J. Perisic, M. Kovacic, H. Kusic, U.L. Stangar, V. Marin, A.L. Bozic, The comparative analysis of UV-C/H_2O_2 and UV-A/TiO_2 processes for degradation of diclofenac in water, React. Kinet. Mech. Cat., 118 (2016) 451–462.
[37] P.K.J. Robertson, J.M.C. Robertson, D.W. Bahnemann, Removal of microorganisms and their chemical metabolites from water using semiconductor photo catalysis, J Hazard Mater., 211–212 (2012) 161–171.
[38] T. Fotiou, T.M. Triantis, T. Kaloudis, A. Hiskia, Evaluation of the photo catalytic activity of TiO_2 based catalysts for the degradation and mineralization of cyanobacterial toxins and water off-odor compounds under UV-A, solar and visible light, Chem. Eng. J., 261 (2015) 17–26.
[39] U.I. Gaya, Heterogeneous photo catalysis using inorganic semiconductor solids, Springer, Heidelberg, Germany, 2014.
[40] L. Wojnárovits, T. Pálfi, E. Takács, Kinetics and mechanism of azo dye destruction in advanced oxidation processes, Radiat. Phys. Chem., 76 (2007) 1497–1501.
[41] C. Luo, H. Wang, W. Dong, X. Zhang, Theoretical investigation on the mechanism of the OH-initiated degradation process of Reactive Red 2 azo dye, RSC Adv., 7 (2017) 41799–41811.
[42] M.J. Farré, M.I. Franch, J.A. Ayllón, J. Peral, X. Domènech, Biodegradability of treated aqueous solutions of biorecalcitrant pesticides by means of photo catalytic ozonation, Desalination, 211 (2007) 22–33.
[43] D.J. Perisic, A. Belet, H. Kusic, U.L. Stangar, A.L. Bozic, Photo catalytic treatment of diclofenac in water; comparison of slurry and immobilized processes, Desal. Water Treat., 81 (2017) 170–185.
[44] S. Salaeh, M. Kovacic, D. Kosir, H. Kusic, U.L. Stangar, D.D. Dionysiou, A.L. Bozic, Reuse of TiO_2-based catalyst for solar driven water treatment; thermal and chemical reactivation, J. Photochem. Photobiol. A., 333 (2017) 117–129.
[45] M. Kovacic, N. Kopcic, H. Kusic, U.L. Stangar, D.D. Dionysiou, A.L. Bozic, Reactivation and reuse of TiO_2-SnS_2 composite catalyst for solar driven water treatment, Environ. Sci. Poll. Res., 25 (2018) 2538–2551.
[46] N. Miranda-García, S. Suárez, M.I. Maldonado, S. Malato, B. Sánchez, Regeneration approaches for TiO_2 immobilized photo catalyst used in the elimination of emerging contaminants in water, Catal. Today, 230 (2014) 27–34.
[47] V.G. Gandhi, M.K. Mishra, P.A. Joshi, A study on deactivation and regeneration of titanium dioxide during photo catalytic degradation of phtalic acid, J. Ind. Eng. Chem., 18 (2012) 1902–1907.

Supplementary material

Table S1
The composition of original fly ash sample (FA0)

Constituent	SiO_2	$CaO/CaCO_3$	Al_2O_3	Fe_2O_3	SO_3	K_2O	MgO
Content (%)	42.01	24.30	20.31	5.55	2.37	2.35	1.20

– TiO_2, Na_2O, P_2O_5, CuO < 1%
– SrO, WO_3, MnO, Cr_2O_3, ZnO, NiO, PbO; in traces

Table S2
Model equations of derived RSM models for RR45 removal by solar/TiO_2 and solar/TiO_2-FA during initial dark period and total

Process	Model #	Model equation
Adsorption on TiO_2	M1	$Y = 2.60 - 1.05 \times X_1 + 0.92 \times X_2 - 0.25 \times X_1 \times X_2 - 0.67 \times X_{12} - 0.78 \times X_{22}$
Adsorption on TiO_2-FA	M2	$Y = 2.04 - 1.10 \times X_1 + 0.60 \times X_2 - 0.50 \times X_1 \times X_2 - 0.25 \times X_{12} - 0.69 \times X_{22}$
Solar/TiO_2	M3	$Y = 39.25 - 19.71 \times X_1 + 20.50 \times X_2 - 16.58 \times X_1 \times X_2 - 4.92 \times X_{12} - 10.56 \times X_{22}$
Solar/TiO_2-FA	M4	$Y = 13.06 - 18.99 \times X_1 + 18.66 \times X_2 - 16.61 \times X_1 \times X_2 + 10.09 \times X_1 2 + 3.09 \times X_{22}$

Table S3
Analysis of variance (ANOVA) of the RSM models M1 and M3 predicting RR45 removal by solar/TiO_2 during initial dark period and total

Factor (coded)	Statistical analysis									
	SS		df		MSS		F		p	
	M1	M3	M1	M3	M1	M3	M1	M3	M1	M3
Model	25.77	11704.16	5	95	5.15	2340.83	135.34	52.10	<0.0001*	<0.0001*
X_1	12.46	4360.62	1	1	12.46	4360.62	327.26	97.05	<0.0001*	<0.0001*
X_{12}	1.25	67.65	1	1	1.25	67.65	32.89	1.51	0.0002*	0.2479
X_2	9.12	4503.79	1	1	9.12	4503.79	239.39	100.24	<0.0001*	<0.0001*
X_{22}	1.76	318.92	1	1	1.76	318.92	46.11	7.10	<0.0001*	0.0237*
$X_1 \times X_2$	0.50	2231.28	1	1	0.50	2231.28	13.24	49.66	0.0045*	<0.0001*
Residual	0.38	449.30	10	10	0.038	44.93				
Total	26.15	12153.46	15	15						

*p < 0.05 are considered as significant.

Table S4
Analysis of variance (ANOVA) of the RSM models M2 and M4 predicting RR45 removal by solar/TiO2-FA during initial dark period and total

Factor (coded)	Statistical analysis									
	SS		df		MSS		F		p	
	M2	M4	M2	M4	M2	M4	M2	M4	M2	M4
Model	21.17	10534.22	5	5	4.23	2106.84	49.08	186.42	<0.0001*	<0.0001*
X_1	13.67	4048.31	1	1	13.67	4048.31	158.42	358.20	<0.0001*	<0.0001*
X_{12}	0.18	284.09	1	1	0.18	284.09	2.06	25.14	0.1813	0.0005*
X_2	3.82	3733.09	1	1	3.82	3733.09	44.26	330.31	<0.0001*	<0.0001*
X_{22}	1.37	27.33	1	1	1.37	27.33	15.91	2.42	0.0026*	0.1510
$X_1 \times X_2$	2.03	2240.06	1	1	2.03	2240.06	23.50	198.20	0.0007*	<0.0001*
Residual	0.86	113.02	10	10	0.086	11.30				
Total	22.04	10647.24	15	15						

*p < 0.05 are considered as significant.

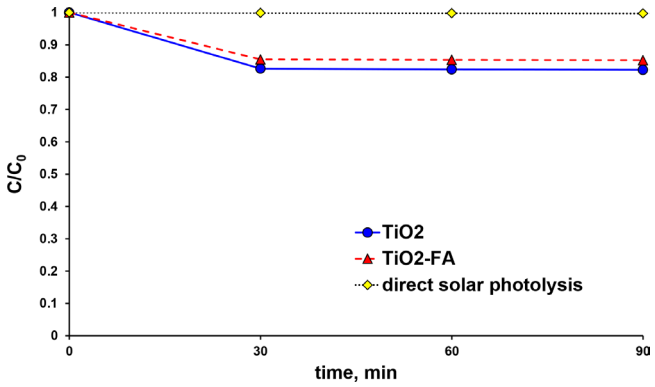

Fig. S1. Adsorption of RR45 dye onto TiO_2 and TiO_2-FA in the dark (pH 3, γ(RR45) = 30 mg L^{-1}, γ(TiO_2) = 1.6 g L^{-1}, γ(TiO_2-FA) = 1.6 g L^{-1}) and degradation of RR45 by direct solar photolysis (pH 3, γ(RR45) = 30 mg L^{-1}).

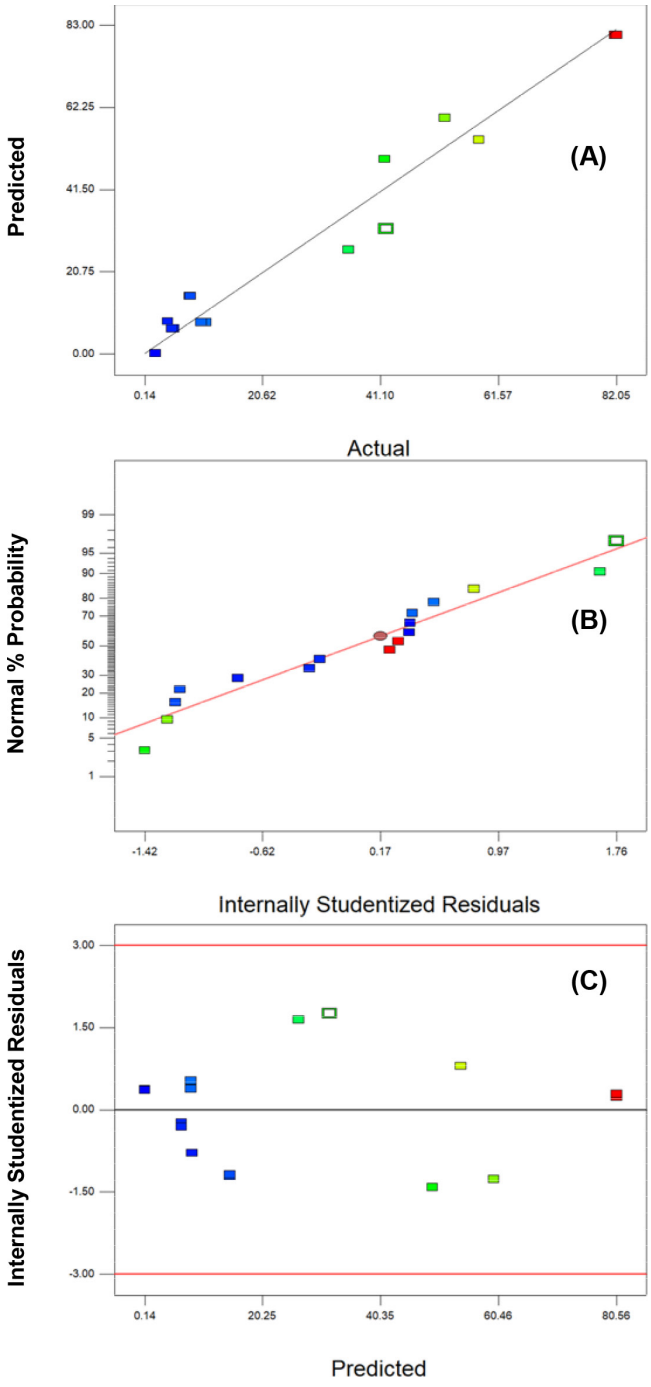

Fig. S2. Residual diagnostics of model M3 for the prediction of the total removal of RR45 by solar/TiO_2 process: (A) observed vs. predicted plot, (B) normal probability plot, and (C) internally studentized residuals vs. predicted values plot.

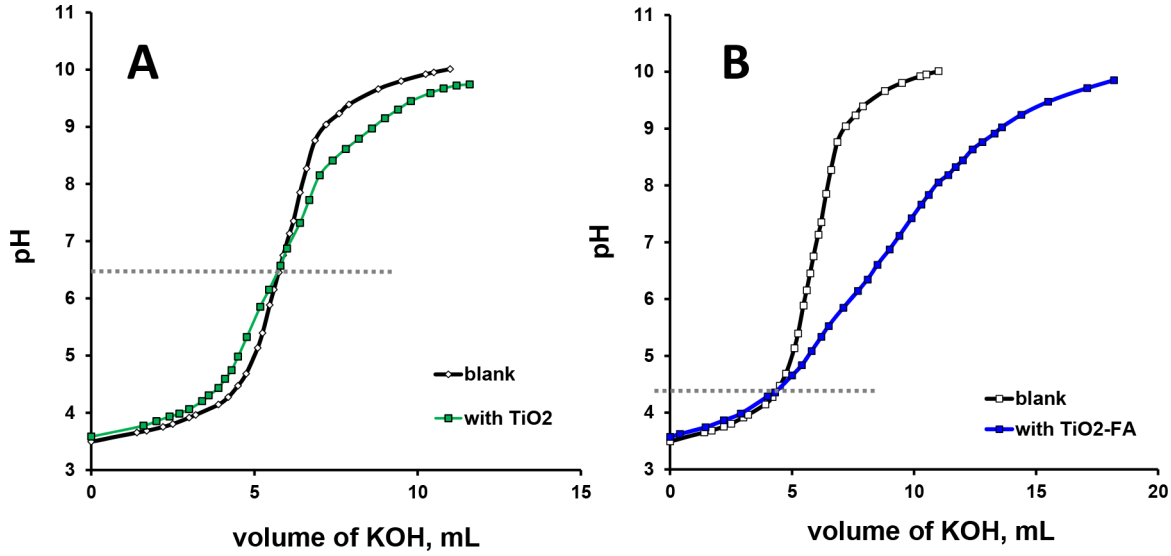

Fig. S3. Determination of point of zero charge (PZC) for TiO_2 (A) and TiO_2-FA (B).

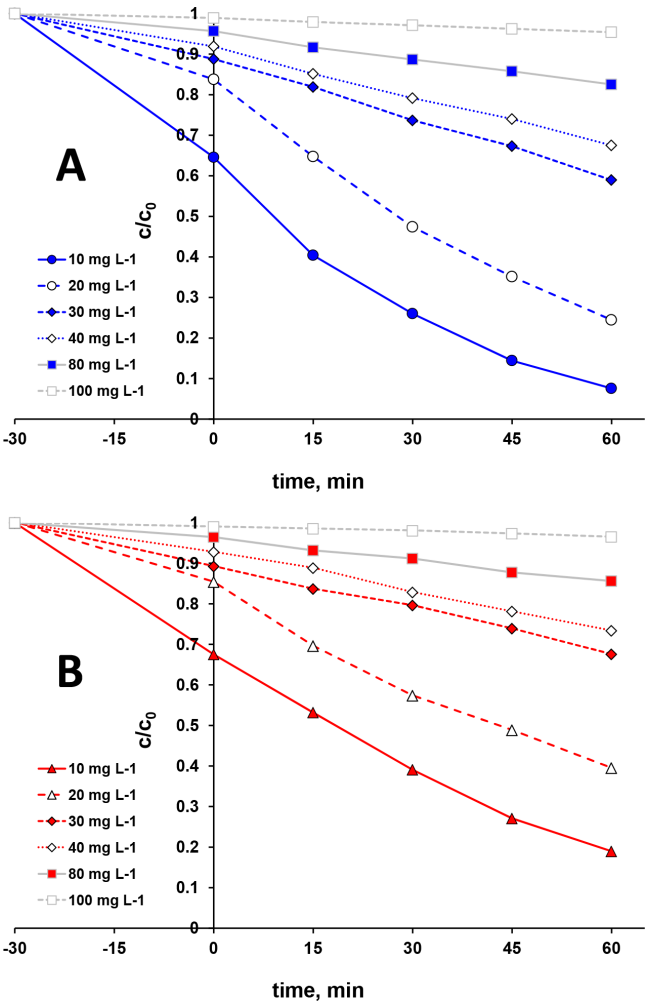

Fig. S4. The influence of initial RR45 concentration on the effectiveness of solar/TiO_2 (A) and solar/TiO_2-FA (B) (pH 4.8, γ(RR45) = 30 mg L^{-1}, γ(TiO_2) = 1.6 g L^{-1}, γ(TiO_2-FA) = 1.6 g L^{-1}).